ERA report series

17 Capturing Tropical Instability Waves in the ECMWF Coupled Reanalysis System

Eric de Boisséson, Patrick Laloyaux and Magdalena Balmaseda

Series: ERA Report Series

A full list of ECMWF Publications can be found on our web site under:

http://old.ecmwf.int/publications/

Contact: library@ecmwf.int

© Copyright 2015

European Centre for Medium Range Weather Forecasts
Shinfield Park, Reading, Berkshire RG2 9AX, England

Literary and scientific copyrights belong to ECMWF and are reserved in all countries. This publication is not to be reprinted or translated in whole or in part without the written permission of the Director. Appropriate non-commercial use will normally be granted under the condition that reference is made to ECMWF.

The information within this publication is given in good faith and considered to be true, but ECMWF accepts no liability for error, omission and for loss or damage arising from its use.

Abstract

The European Centre for Medium-Range Weather Forecasts (ECMWF) has developed a prototype of ocean-atmosphere coupled assimilation system that will be used for 20th century reanalysis experiments. This system has been run over a two-year period using a century-reanalysis configuration. The ability of the system to capture intraseasonal coupled processes such as Pacific Tropical Instability Waves (TIWs) is evaluated against observations and an atmosphere-only reanalysis. The coupled reanalysis shows to be an improvement over the atmospheric reanalysis as it is able to capture these tropical instabilities with similar characteristics as the observed state except for relatively weak amplitudes. Experiments show that alternative methods to constrain the air-sea interface of the system may improve the representation of the tropical instabilities in the analysis fields.

1 Introduction

ERA-CLIM2 is the extension of the ERA-CLIM project that aims at building a sustainable reanalysis capability for European climate services. Within the original ERA-CLIM project, the European Centre for Medium-Range Weather Forecasts (ECMWF) produced a century atmospheric reanalysis (called ERA20C) that only assimilated surface conventional observations [*Poli et al.*, 2013]. In this experiment, the atmosphere was forced at its lower boundary by a monthly Sea Surface Temperature (SST) and Sea Ice product, called HadISST2, provided by the Hadley Centre [*Rayner et al*, 2003]. Such atmospheric forcing is missing the submonthly from the ocean surface. At these timescales, coupled ocean-atmosphere processes such as Madden-Julian Oscillation or Tropical Instability Waves (TIWs) are known to play a significant role in various aspects of the climate system [*Vitart and Molteni*, 2010; *Hashizume et al.*, 2001; *Ham and Kang*, 2009]. Such processes can be captured by ocean-atmosphere coupled models [*Inness and Slingo*, 2003; *Seo et al.*, 2007], but, due to rapid model drift, may be far from the observed state of the system.

Within the ERA-CLIM2 project, ECMWF has been developing a prototype of coupled ocean-atmosphere reanalysis system called CERA (for Coupled ECMWF ReAnalysis). One of the main challenges when building such system is to constrain the coupled model as close as possible to observations while allowing it to capture coupled ocean-atmosphere processes and thus provide climate states that are as consistent as possible. A first version of the CERA system has been built and several short reanalysis experiments (typically 2-3 months) have been conducted [*Laloyaux et al.*, 2015]. Results show that the CERA system represents better the coupled state, reduces the background and analysis error with respect to ocean temperature observations and improves the atmospheric temperature representation over the Tropics.

One of the deliverables of the ERA-CLIM2 project is the production of a coupled ocean-atmosphere reanalysis over the 20th century using a similar assimilation strategy as for ERA20C. The CERA system has been configured for ERA-20C-like experiments and several 2-year experiments have been conducted. This study focuses on the ability of the CERA system to produce analysis fields that intraseasonal coupled processes such as TIWs in the Pacific Ocean. Comparisons with both ERA20C analysis fields and satellite observations of SST and surface wind are conducted. We also give insights into the impact of the assimilation of subsurface ocean observations and of the SST constraint on the quality and the realism of the TIWs in the analysis.

Section 2 of this report describes the CERA system and the representation of the TIWs in the different experiments. The results are discussed and our conclusions are drawn in Section 3.

2 The CERA system experiments

2.1 Description of the system

ECMWF has been developing a coupled assimilation system called CERA (for Coupled ECMWF ReAnalysis) that incorporates both ocean and atmospheric observations into a coupled ocean-atmosphere model using an incremental variational approach. The CERA system is based on the ECMWF coupled model that includes the IFS atmospheric model (cycle 40R1), the WAM wave model and the NEMO v3.4 ocean model. The ocean-atmosphere coupling is sequential with a one-hour time step. The resolution of the atmosphere is T159L137 (around 1.125 degree horizontal grid with 137 vertical levels). The ocean model uses the ORCA1 grid (roughly a 1-degree horizontal resolution) with 42 vertical levels and a first layer of 10 meters. The horizontal resolution of the wave model is 1.5 degree with a wave spectra discretized using 12 directions and 25 frequencies.

The CERA system assimilates simultaneously ocean and atmospheric observations from a common 24-hour assimilation window (Figure 1). The outer loop integrates the coupled model, producing a 4-dimensional state estimate and observation misfits. The inner loop solves in parallel a linearized version of the variational formulation for the ocean and the atmospheric components. The coupled ocean-atmosphere analysis is carried forward in time by the coupled model to the next assimilation window. In the current implementation, the CERA system computes two outer iterations to produce the ocean and atmospheric analysis, which allows the observations from one component to affect the other component [*Laloyaux et al*, 2015]. The model SST is relaxed toward observation-based SST analysis to avoid the rapidly-growing bias at the air-sea interface of the coupled model (see Equation A.1.1 of the Appendix for more details).

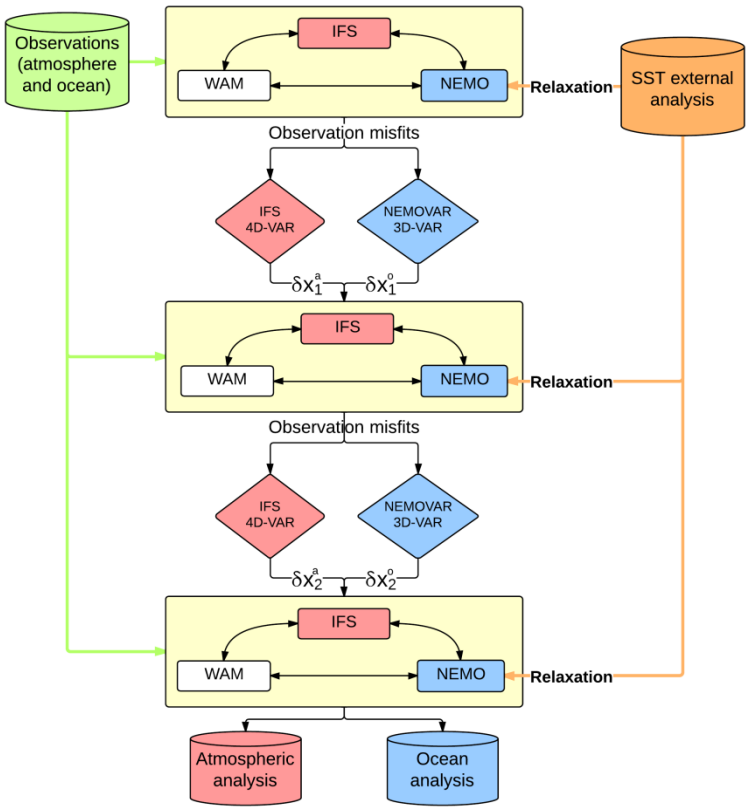

Figure 1 *Schematic diagram of the CERA coupled assimilation system. Yellow boxes represent model integrations, while diamonds represent increment computations. This diagram illustrates the computation of two outer iterations of the incremental variational method.*

The CERA system has been run over the period 2009-2010 for the purposes of the ERA-CLIM2 project. Like ERA20C, the CERA system assimilates conventional surface atmospheric observations only (mean sea-level pressure and surface winds). The ocean component assimilates subsurface observations from temperature and salinity profiles, while the ocean-atmosphere interface is relaxed toward the SST and Sea-Ice from HadISST2 with a timescale of 2 to 3 days ($\lambda = 200 W m^{-2}$ in Equation A.1.1). As this experiment is using the standard configuration of the CERA system, it is referred to as CERA. An additional experiment is conducted where the assimilation of subsurface observations is switched off in order to evaluate its impact and to simulate the poor ocean sampling of the early 20th century. This experiment is referred to as CERA-noODA (for no Ocean Data Assimilation). In the following, we compare our CERA experiments to observations and to ERA20C (where the SST is prescribed).

2.2 Pacific Tropical Instability Waves in the CERA system

The general performance of the CERA system has been evaluated in *Laloyaux et al.* [2015]. In this section, we focus on the ability of the system to represent intraseasonal coupled processes. We aim to show the benefit of coupling atmosphere and ocean when compared to an atmosphere-only analysis like ERA20C. Satellite observations are used to give insight into how close/far those products are from what we know of reality. Because of the relatively short length of the experiments, the westward-propagating TIWs visible in the eastern tropical Pacific (mainly in the 1˚S-3˚N band) are chosen as case study. These

waves have wavelengths of 1000-2000 km, periods of 20-30 days, and phase speeds of about 0.5 m s^{-1} [*Willet et al*, 2006].

2.2.1 Tropical Instability Waves: spectral analysis

A wavenumber-frequency spectral analysis is conducted on the SST fields from the different datasets following the method described in *Wheeler and Kiladis* [1999]. This method has shown efficiency in detecting ocean equatorial waves such as the TIWs [*Shinoda et al*., 2009 and *Shinoda,* 2012]. Linear equatorial waves being either anti-symmetric or symmetric about the equator, an antisymmetric-symmetric decomposition is performed over SST data in the 5˚S-5˚N latitudinal band [*Wheeler and Kiladis*, 1999]. The resulting power-spectra are analysed by analogy to the equatorial wave theory [*Pedlovsky*, 2003].

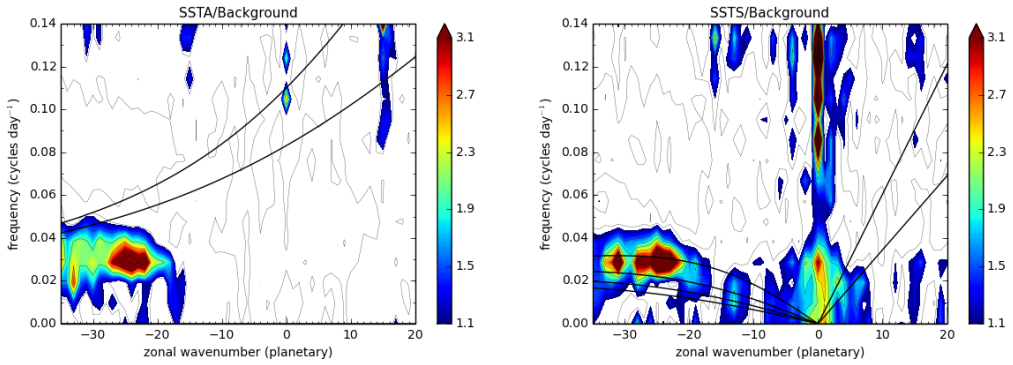

a) Power-spectrum TMI SST

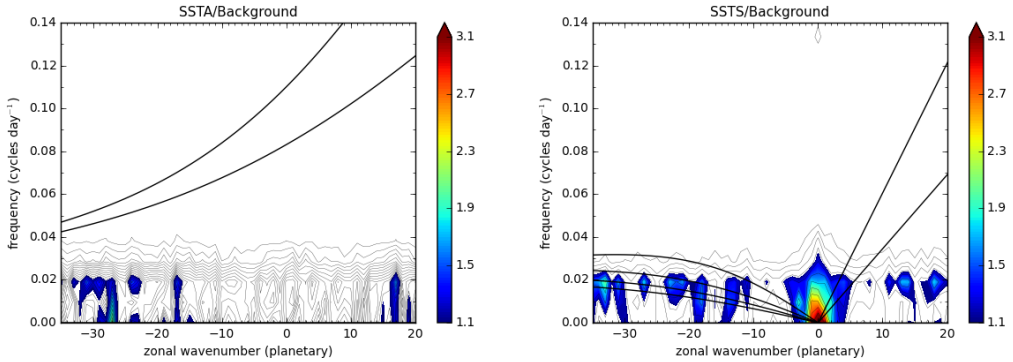

b) Power-spectrum HadISST2 (ERA20C)

Figure 2 Zonal wavenumber-frequency power spectra of SST (divided by the background) for both anti-symmetric (left panel) and symmetric components (right panel): a) TMI SST, b) HadISST2 (used to force ERA20C). Contour interval is 0.1 and shading begins at a value of 1.1 for which the spectral signatures are statistically significantly above the background at the 95% level (see in Wheeler and Kiladis [1999]). The curves on the left panel indicate mixed Rossby-gravity (Yanaï) waves dispersion relation for equivalent depth of 0.8 m and 0.26 m [Shinoda, 2012]. The straight lines on the right panel indicate the first baroclinic Kelvin waves for equivalent depths of 0.8 m and 0.26 m. The curves are Rossby wave dispersion relation for the first 4 meridional modes for an equivalent depth of 0.8 m [Shinoda et al, 2009].

The SST observations from the Tropical Microwave Imager (or TMI [*Gentemann et al*, 2004]) show a prominent spectral signal around negative wave-numbers 25 to 30 (1300-1600km wavelength) and frequencies centered around 0.03 cycle per day (33-day period) on both symmetric and anti-symmetric components (Figure 2a). The spectral peak for the symmetric component is close to the dispersion curve of the first meridional mode equatorial Rossby wave, which is consistent with results from *Shinoda et al* [2009]. These wave characteristics correspond to what we know from TIWs. The spectral signal corresponding to the 17-day TIW [*Shinoda*, 2012] cannot be seen on the anti-symmetric component. This may be due to the fact that we consider only 2 years of data for this spectral analysis.

The monthly HadISST2 product used to force the ERA20C atmospheric analysis does not show any spectral signal corresponding to TIWs (Figure 2b). Its temporal resolution is too coarse to capture such signal. The atmosphere from ERA20C will therefore not see the oceanic TIW signal. CERA uses the information from HadISST2 in order to constrain the ocean-atmosphere interface of the coupled model. When ocean subsurface observations are not assimilated in CERA-noODA, the TIW spectral signal is slightly off the first meridional mode equatorial Rossby wave curve on the symmetric component (Figure 3a, right panel). It is centered over wavenumbers higher than 30 and a period of 26 days. The spectral signal is much weaker on the anti-symmetric component (Figure 3a, left panel). Assimilating ocean observations in CERA corrects the spectral signal of the TIWs towards the observed state (Figure 3b).

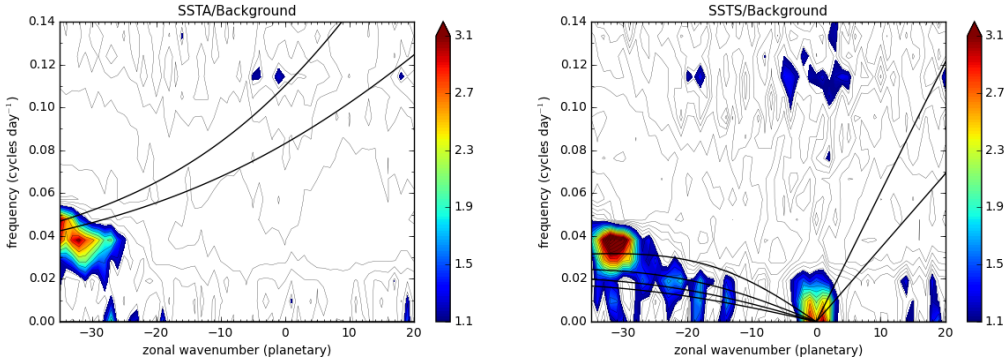

a) Power-spectrum CERA-noODA

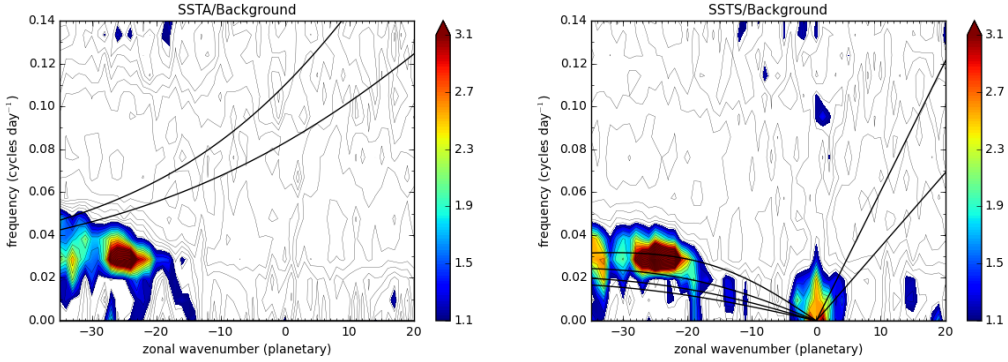

b) Power-spectrum CERA

Figure 3 Same as Figure 2 but for CERA-noODA (a) and CERA (b).

The wavenumber-frequency analysis shows that the ocean component of the CERA system can capture a TIW signal with correct spectral characteristics that will be transferred to the atmospheric component. Such signal not being captured by HadISST2, the atmosphere of ERA20C will not be exposed to the oceanic forcing from TIWs.

2.2.2 Tropical Instability Waves: ocean-atmosphere coupling

The TIWs are characterized by a very close relationship between SST and wind anomalies. In the following, SST and surface wind stress fields are zonally high-passed filtered to attenuate wavelength longer than 2000km as in *Chelton et al.* [2001]. A temporal band-pass filter (centred on the window 10 to 60 days) is also applied to focus on the period of the TIWs. The TIW signal of 2009 is unfortunately very weak due to El Nino conditions [*Kim et al*, 2011]. The switch to La Nina conditions in spring 2010 is favorable to the formation of TIWs that are indeed strong from May 2010. TIWs are better detected north of the Equator between 1˚N and 3˚N. In the following, we focus on the TIW signal detected in 2010 at 1˚N in the Pacific Ocean between 90˚W and 180˚W using longitudinal Hovmöller diagrams and lag correlations.

SST observations from TMI show a westward propagation of a signal associated with TIWs with values ranging between $\pm$2K (Figure 4a). The propagation speed is estimated by hand (see green slopes on Figure 4a) and varies from 0.48 m s^{-1} at the beginning of the TIW season (May-July) to 0.62 m s^{-1} afterwards (up to December). As shown on Figure 2b, the monthly HadISST2 product used to force ERA20C is not able to capture the TIW signal (Figure 4b). The CERA system constrained by HadISST2 is able to capture the spectral signal of TIWs (Figure 3). When no ocean subsurface observations are assimilated, CERA-noODA shows a TIW signal propagating westward from June onward with a speed of 0.63 m s^{-1} (Figure 4c). This is an improvement when compared to ERA20C. Insights into the phase relationship between the model TIWs and the observed signal are provided through the lag-correlation between SST (wind stress) time series from both datasets at 1˚N (Figure 6). When the lag is negative (positive) the model is leading (lagging) observations. The SST signal from CERA-noODA leads the observed signal by a few days (Figure 6a). When assimilating the subsurface observations in CERA, the TIW signal keeps the same propagation speed as in CERA-noODA but shows an improved phasing with the observations (Figure 4d and Figure 6b), which is consistent with what we learnt from the spectral analysis (Figure 3b). The SST anomalies in CERA are however substantially weaker than in CERA-noODA and in the observations.

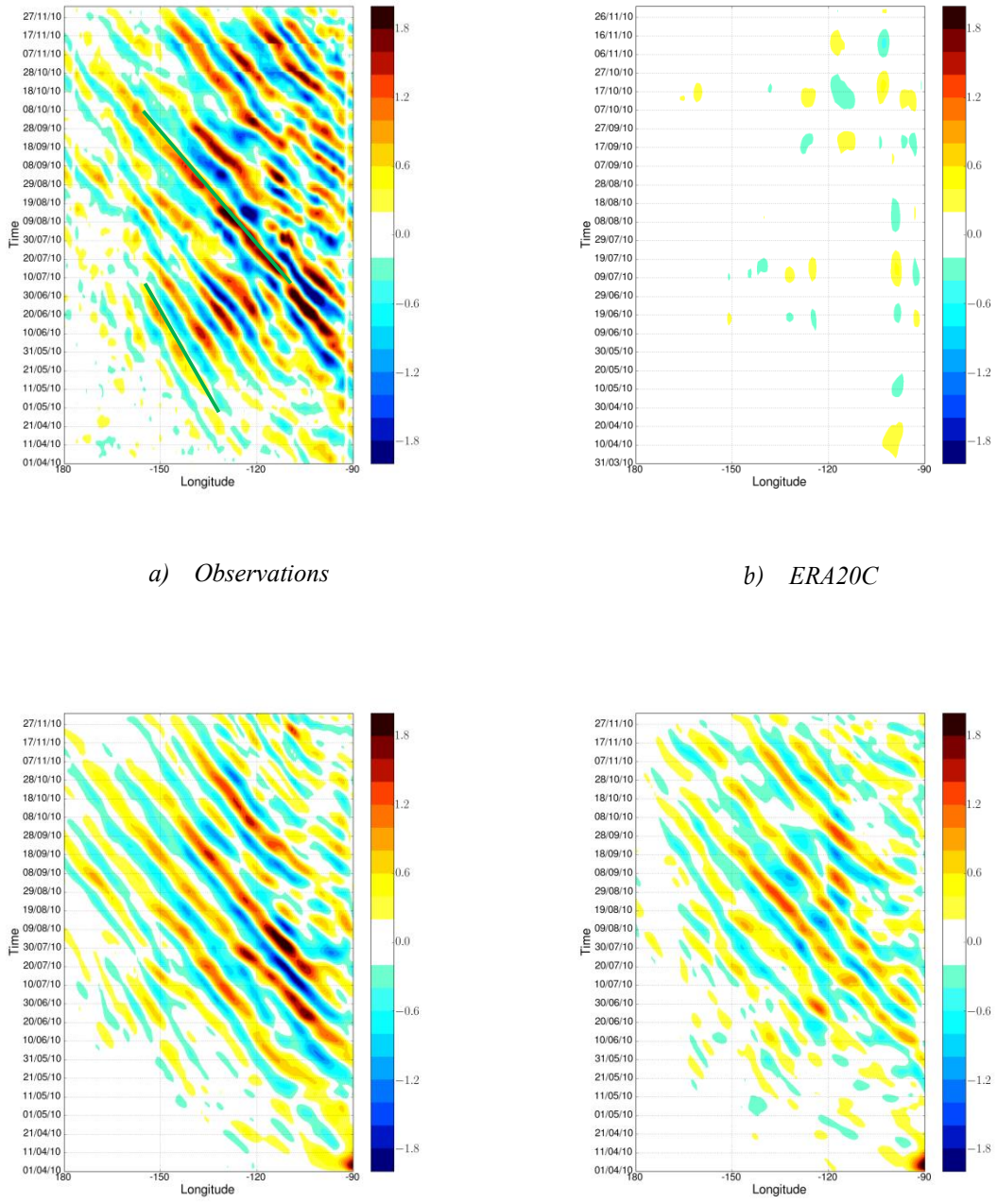

a) Observations

b) ERA20C

c) CERA-noODA

d) CERA

Figure 4 Longitudinal hovmoller diagrams at 1˚N in the Equatorial Pacific (90-180˚W) of the high-pass filtered SST from April to December 2010 in a) observations from TMI, b) ERA20C (HadISST2), c) CERA-noODA and d) CERA. The green straight lines on panel a) are used for our handmade estimate of the TIW propagation speed.

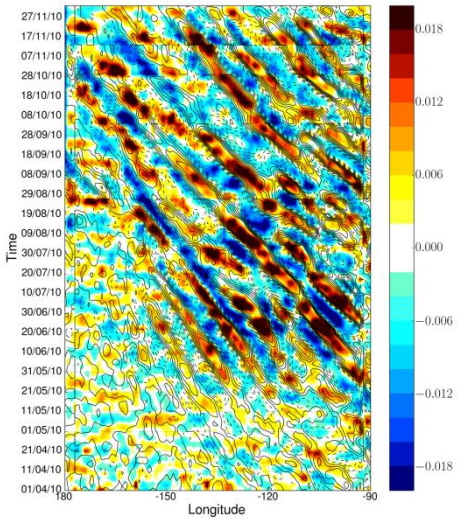

a) Observations

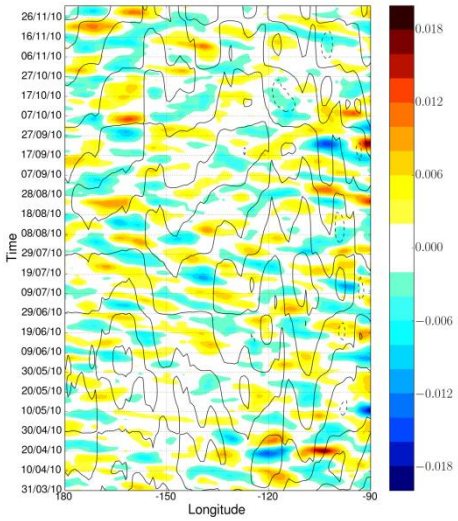

b) ERA20C

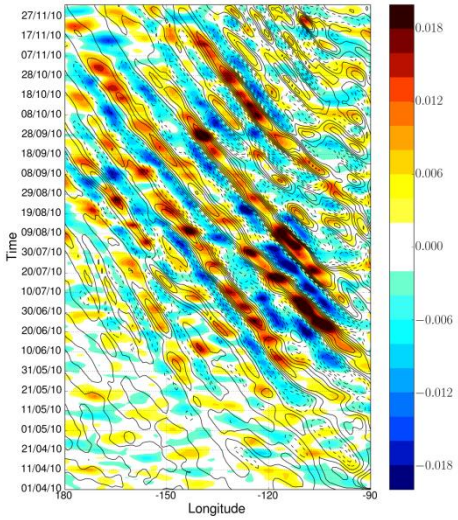

c) CERA-noODA

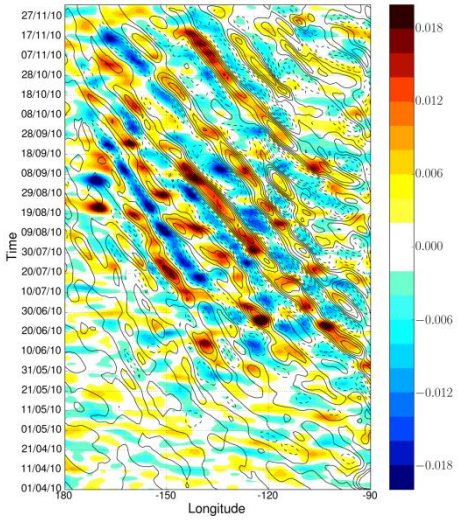

d) CERA

Figure 5 Longitudinal hovmoller diagrams at 1˚N in the Equatorial Pacific (90-180˚W) of the high-pass filtered wind stress from April to December 2010 in a) observations from ASCAT, b) ERA20C, c) CERA-noODA and d) CERA. The wind stress is superimposed on the contours (interval of 0.25K) of SST shown in Figure 4.

Analyzing scatterometer data from the A-Scatterometer (or ASCAT, using the reprocessed data from *Bentamy et al.* [2012]) shows that the surface wind stress is sensitive to the ocean TIW signal. A wind stress signal with amplitudes varying between ±0.02 N m^{-2} propagates westward (Figure 5a). The lag-correlation between SST and wind stress time series at 1˚N (Figure 10a) is centered on the 0 lag, showing that both parameters are in phase. ERA20C, being forced by monthly SST, produces a wind stress field that does not capture the TIW signal (Figure 5b), suggesting that the ocean is forcing the wind in that case. The atmospheric component of CERA is capturing a TIW wind signal. In CERA-noODA, the wind stress is in phase with the SST (Figure 10b) but out of phase with the observed state (Figure 6c). Adding the ocean assimilation in CERA reduces the intensity of the wind stress signal but its phase relationship with the observed state is more centered on the 0 lag (Figure 5d, Figure 6d and Figure 10c).

These simple results show that, from the point of view of capturing intraseasonal coupled processes, the CERA system is an improvement over ERA20C. In spite of a loss of TIW intensity, assimilating subsurface ocean observations improves the phasing between analysis and observed state in both ocean and atmospheric components.

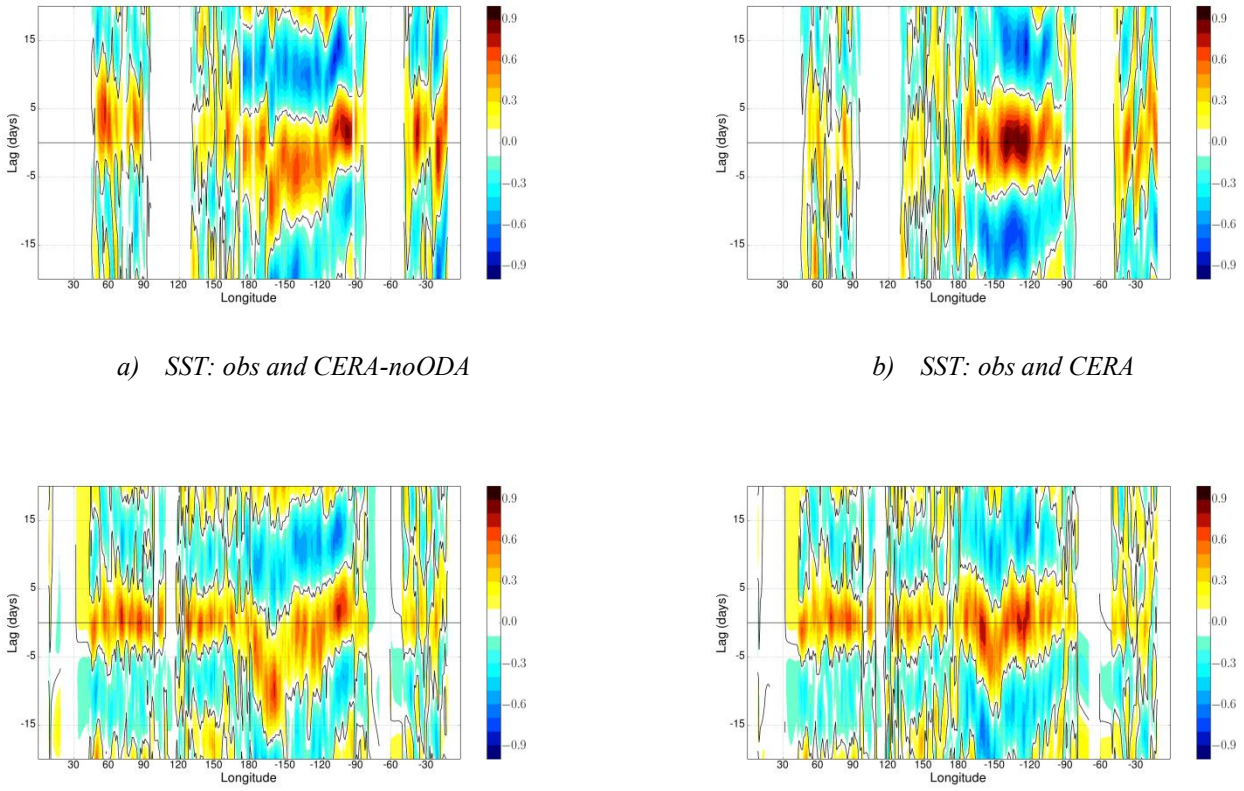

a) SST: obs and CERA-noODA

b) SST: obs and CERA

c) TAU: obs and CERA-noODA

d) TAU: obs and CERA

Figure 6 Lag correlation at 1˚N between the high-pass filtered SST from observations and a) CERA-noODA and b) CERA over the period April-December 2010. c, d) Same as a, b) but for the high-pass filtered wind stress. The 0 lag means that the compared signals are in phase. Negative (positive) lags mean that the model is lagging (leading) the observations.

2.2.3 Constraining the air-sea interface in CERA

In our setup for the CERA system, the air-sea interface is constrained by relaxing the SST toward HadISST2. The correction is applied at every time step (see Equation A.1.1 of the Appendix) and is linearly related to the difference between the instantaneous model SST and HadISST2 (temporally interpolated at the model time step). As mentioned in Section 2.1, the timescale of the constraint in the standard CERA setup is around 2-3 days. Constraining the coupled system interface to monthly observed SST with such timescale is not ideal in the perspective of capturing intraseasonal coupled processes. Our observed SST being a monthly product, a potential alternative would be to relax only the monthly mean of the model SST. A new formula has been tested (see Equation A.1.2 of the Appendix) where the monthly mean of the model SST is relaxed toward HadISST2 with a timescale of 2-3 days ($\lambda_2 = 200 W m^{-2}$ in Equation A.1.2). For stability reasons (see Appendix A.2), the instantaneous SST is still constrained but with a timescale of 25 days ($\lambda_1 = 20 W m^{-2}$ in Equation A.1.2). Two-year experiments of the CERA system have been conducted using this formula with and without assimilating subsurface ocean observations. These experiments are referred to as CERAE (for CERAExperimental) and CERAE-noODA, respectively.

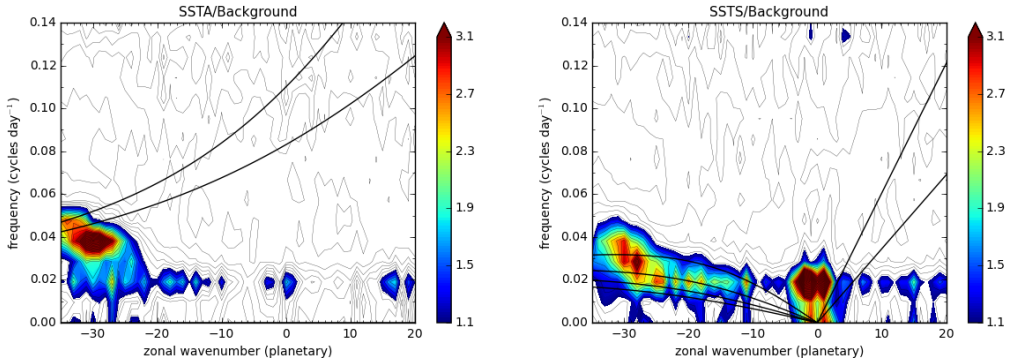

a) Power-spectrum CERAE-noODA

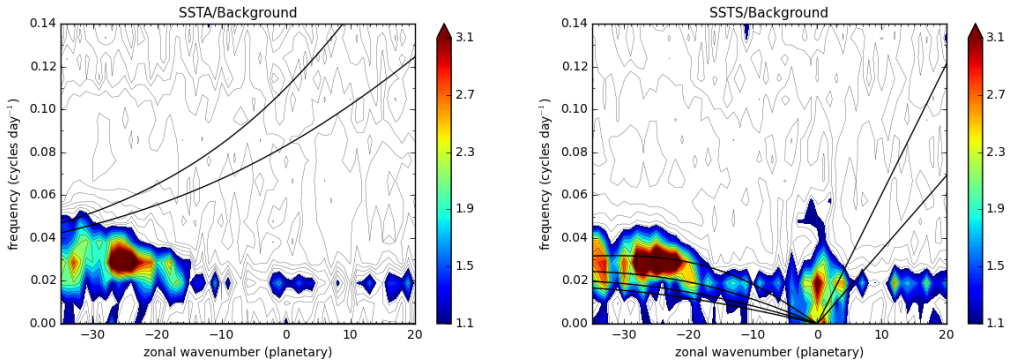

b) Power-spectrum CERAE

Figure 7 Same as Figure 2 but for CERAE-noODA (a) and CERAE (b).

As with the others experiments, a spectral analysis on the SST field is first conducted. When the ocean data assimilation is off in CERAE-noODA, the spectral peak on the symmetric component is more diffuse than in CERA-noODA (Figure 7a to compare to Figure 3a). The spectral signal spans a relatively wide range of wavenumber and frequency corresponding to the first and second modes equatorial Rossby wave. The anti-symmetric component shows a relatively strong spectral signal with wavenumber and frequency corresponding to TIWs. As in CERA, assimilating ocean observations constrains the spectral signals of CERAE SST toward the observed state (Figure 7b to compare to Figure 2a and Figure 3b). The resulting wavenumber-frequency spectrum from CERAE show similar signals as CERA and the observations.

We then focus on the representation of the 2010 TIW propagation and coupled interactions at 1˚N. Without ocean data assimilation, CERAE-noODA shows SST anomalies associated to TIW (Figure 8a) that are more intense, more frequent (one cycle more over the June-November period) and propagate slightly slower (0.55 m s^{-1}) than in CERA (Figure 4c,d). The SST signal from CERAE-noODA is largely out of phase with the observed state (Figure 9a). Assimilating subsurface observations constrains the frequency and the propagation speed (now 0.63 m s^{-1}) of the TIW in CERAE toward the observed state (good phase relationship on Figure 9b) while keeping a more intense signal than in CERA (Figure 8b to be compared to Figure 4d). Wind stress anomalies are in phase with SST both in CERAE-noODA and CERAE (Figure 10d,e). CERAE-noODA is out of phase with the wind observations (Figure 9c). The assimilation of subsurface ocean observations in CERA-E corrects the phase of the wind stress toward the observed state (Figure 9d). The intensity of the wind stress signal in CERAE is closer to the observations than in CERA (Figure 8d to be compared to Figure 5d).

In this context, the new constraint for the air-sea interface is beneficial for capturing intraseasonal ocean-atmosphere processes in the coupled reanalysis. This conclusion is more contrasted if no subsurface ocean observations are available. The new constraint at the interface gives the coupled model a lot more weight, which produces TIW that have different speed and frequency than in the reality of the observations. The standard constraint, though not optimal to capture intraseasonal coupled processes, does a better job in matching the observed state (compare Figure 6a,c and Figure 9a,c) and is presently a safer option for poorly-observed periods.

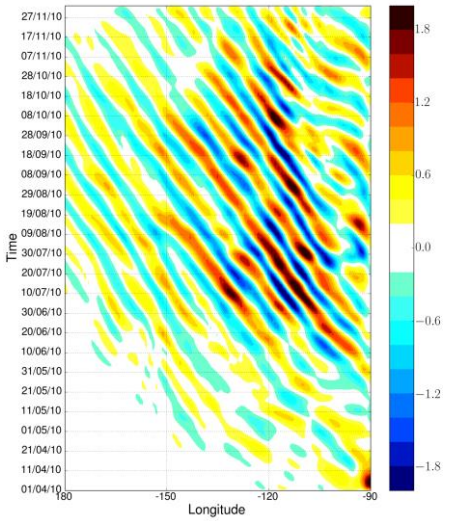

a) SST from CERAE-noODA

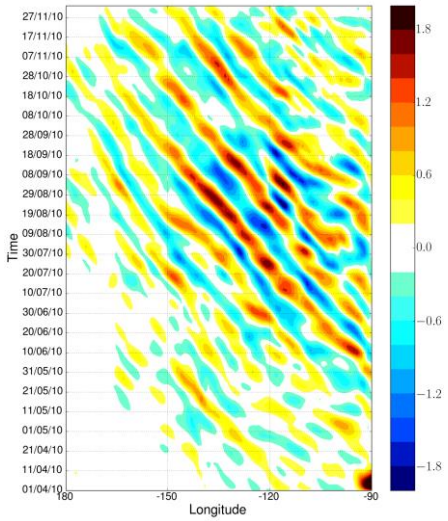

b) SST from CERAE

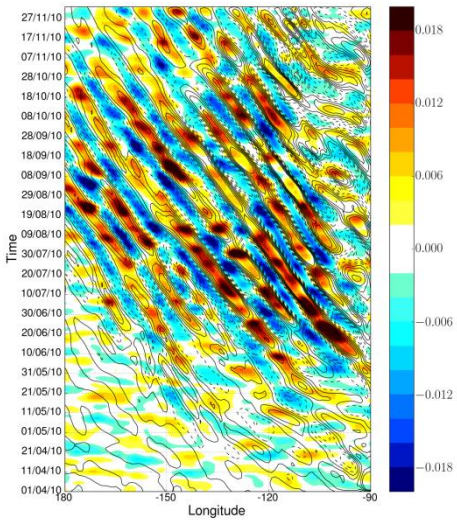

c) Stress from CERAE-noODA

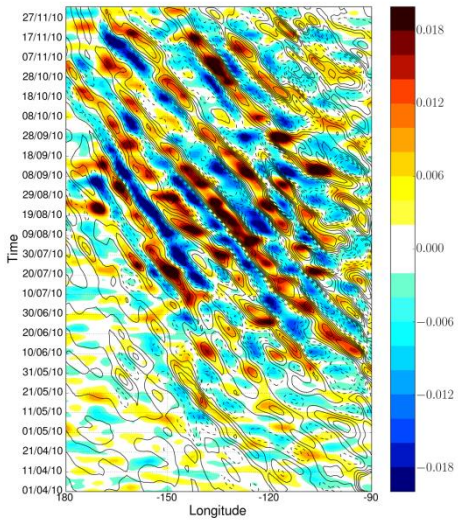

d) Stress from CERAE

Figure 8 Longitudinal hovmoller diagrams at 1˚N in the Equatorial Pacific (90-180˚W) of the high-pass filtered SST from April to December 2010 in a) CERAE-noODA and b) CERAE. c, d) Same as a, b) but for the wind stress.

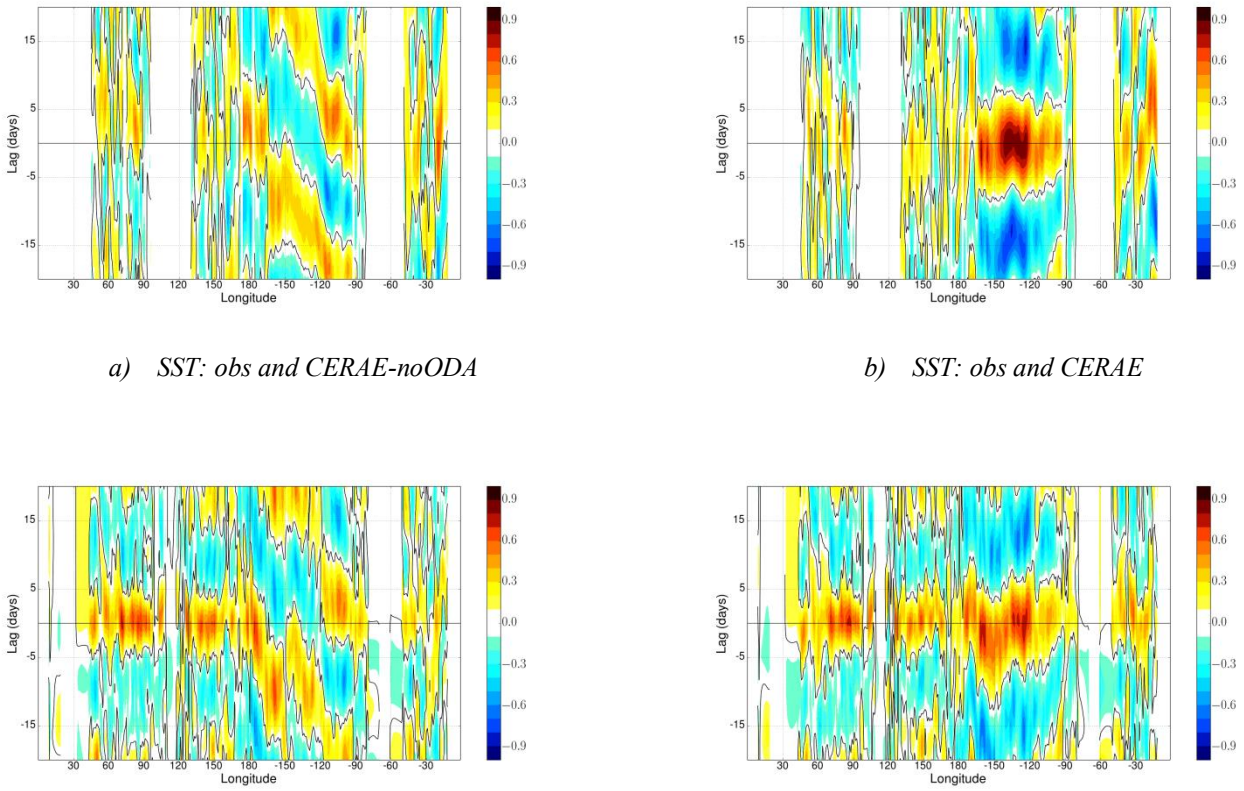

a) SST: obs and CERAE-noODA

b) SST: obs and CERAE

c) TAU: obs and CERAE-noODA

d) TAU: obs and CERAE

Figure 9 Lag correlation at 1˚N between the high-pass filtered SST from observations and a) CERAE-noODA and b) CERAE over the period April-December 2010. c, d) Same as a, b) but for the high-pass filtered wind stress. The 0 lag means that the compared signals are in phase. Negative (positive) lags mean that the model is lagging (leading) the observations.

3 Summary and discussion

The CERA system is an ocean-atmosphere coupled reanalysis system that is being developed at ECMWF within the ERA-CLIM2 project. The CERA system will be used to conduct a coupled reanalysis over the 20th century in a similar way as ERA20C, the century atmosphere-only reanalysis at the core of the first ERA-CLIM project. Several two-year runs of the CERA system are analysed to assess the benefits of coupling in the context of capturing intraseasonal coupled processes in the reanalysis product. Given the short period covered by our experiments, this study focuses on how the different systems (CERA and ERA20C) capture the TIW signals and their coupled interactions.

Observations show TIWs as a wave-like propagation of a SST signal toward the eastern Pacific. This signal is in phase with the surface wind stress from scatterometer. The TIW-related wind signal is not represented in the atmosphere-only ERA20C reanalysis. ERA20C assimilates only sea level pressure and wind observations over the ocean - including the wind observations from the TAO array. ERA20C uses lower boundary conditions from the monthly analyses of SST and Sea-ice from HadISST2 that do not capture the TIW spectral signal. The absence of TIWs in ERA-20C has at least two direct

implications. First, as argued in the literature [*Chelton et al*., 2004; *Seo et al*, 2007], the TIW signature in the surface wind detected in the observations is forced by the ocean. Second, the assimilation method in ERA20C cannot reproduce the TIW-induced wind signal captured by the TAO wind observations. Understanding better the second statement requires additional investigations that are beyond the scope of this study.

The CERA coupled reanalysis assimilates the same observations as ERA20C and its air-sea interface is constrained toward the monthly HadISST2 analysis. The CERA analysis fields show TIWs with similar spectral characteristics, phase and propagation speed as the observations for both the SST and the surface wind stress. The CERA system is an improvement over ERA20C in that respect. Comparing the results from both CERA and ERA20C analysis fields suggests that the atmosphere is responding to the presence of the oceanic TIW signal. While assessing the impact of the ocean dynamics in the atmosphere needs further investigations, our results show that capturing the intraseasonal SST variability is crucial to represent the atmospheric response to TIWs. The way the air-sea interface is constrained in the CERA system is therefore an important aspect of the CERA system.

As mentioned above, the standard CERA setup for century reanalysis constrains the instantaneous model SST towards a monthly SST analysis. This method is straightforward but could be detrimental when looking at submonthly to seasonal coupled processes. An attempt to give more weight to the coupled model by constraining the monthly average of the model SST toward the monthly SST analysis has been conducted. The resulting TIWs show obvious ocean-atmosphere feedback and intensities that are more realistic than in the standard CERA setup. Without assimilation of ocean subsurface observations, the TIW spectral characteristics and propagation however differ substantially from the reality of the observations. The standard CERA setup is more conservative in that respect. When given more weight, the coupled model thus shows more variability at the air-sea interface but this variability translates into TIW-like processes that do not match the observations. The future increase in both horizontal and vertical resolution of the ocean component of the coupled system may improve the representation of TIWs. In the meantime, the assimilation of ocean subsurface observations is essential to constrain the near surface characteristics of the CERA system towards the observed state. The need of subsurface observations could therefore be problematic for periods where the ocean sampling is poor (typically the early 20th century). Addressing this issue remains one of the main challenges for the century coupled reanalysis experiment that will be conducted within the ERA-CLIM2 project.

This study reports on the ability of the CERA system to represent the TIW signal. CERA achieves to a certain extent what ERA20C was unable to do. This opens the doors to new questions and investigations. One of the next steps will be to assess the impact of the TIWs on the analysis of atmospheric parameters such as precipitations or heat fluxes. Several studies showed evidences of a significant remote atmospheric response to TIW forcing in the Intertropical Convergence Zone (ITCZ) [*Hashizume et al.*, 2001; *Caltabiano et al.*, 2005; *Wu and Bowman*, 2007]. Following similar line of argument, the experiments presented in this study should allow to assess the vertical and latitudinal extension of the TIW impact. This would give insights on the potential role of the TIW in weather events. *Ham and Kang* [2011] showed improvements in ENSO forecasts including TIWs in their initial conditions. Similar investigations could be conducted using initial conditions from ERA20C and CERA and could be extended to the predictability of important precipitation events or tropical cyclones. A reanalysis system

such as CERA will provide opportunities to understand better the coupling between ocean-atmosphere and its impact on the climate on various temporal and spatial scales.

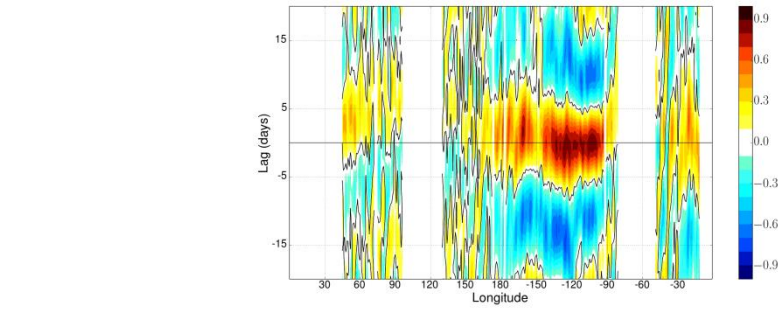

a) SST-TAU observations

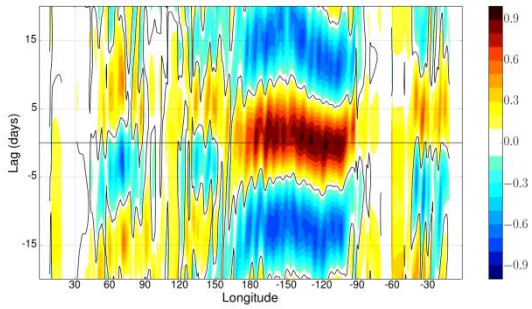

b) SST-TAU CERA-noODA

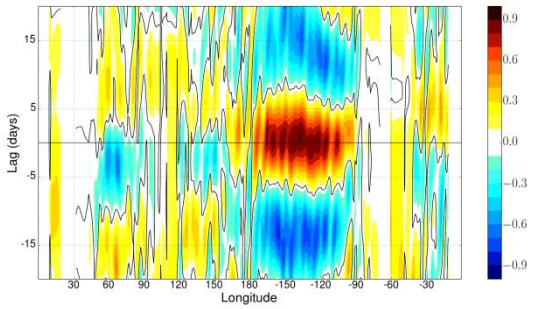

c) SST-TAU CERA

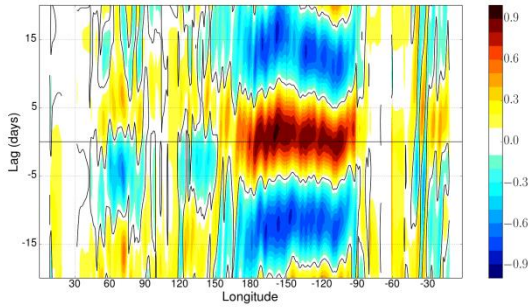

d) SST-TAU CERA-E-noODA

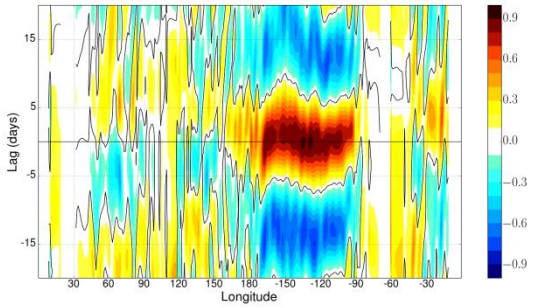

e) SST-TAU CERA-E

Figure 10 Lag correlation at 1°N between the high-pass filtered wind stress and SST over the period April-December 2010 in a) observations (TMI SST/ASCAT wind stress), b) CERA-noODA, c) CERA, d) CERA-E-noODA and e) CERA-E. The 0 lag means that the SST and wind stress are in phase. Negative (positive) lags mean that the wind stress is lagging (leading) the SST signal.

Appendix

A.1 The SST constraint: concept

The SST constraint is part of the ocean component of the coupled model. In uncoupled runs and in the ORAS4 system [*Mogensen et al*, 2013], the SST constraint results in a heat flux correction applied to the first layer of the ocean model. The correction is added to the total heat flux term coming from the atmosphere and then included in the computation of the ocean temperature trend. The SST constraint C_1 depends linearly on the difference X between the temperature at the first vertical level of the ocean grid and observed SST at every time step of the ocean model as in Equation A.1.1. The strength of the constraint is set through a single relaxation coefficient (λ in Equation A.1.1) that can be related to the timescale of the constraint we apply to the first ocean model layer.

$$X = SST_{mod} - SST_{obs}$$

$$C_1 = -\lambda X \qquad \text{(A.1.1)}$$

In coupled mode, such formulation needs a strong relaxation coefficient in order to avoid the rapid drift of the model. A strong relaxation is not ideal as it will inhibit the desirable ocean-atmosphere interactions in the coupled system. A new SST constraint is thus developed to mainly constrain the low-frequency (monthly in the current version) signal and give more freedom to higher frequency.

Here, the low frequency part of the constraint depends on the monthly-averaged difference $\bar{X}$ between the modelled and observed SST:

$$\bar{X} = \overline{SST_{mod}} - \overline{SST_{obs}}$$

As modelled SSTs ahead from the current model time step are not available, the monthly differences only use the 31 days prior to the day to which the time step belongs.

The high frequency signal SST' is estimated as the difference between instantaneous values and monthly average.

$$SST' = SST - \overline{SST}$$

The high frequency part of the constraint depends on the difference X' between the observed and modelled high frequency SST:

$$\begin{aligned} X' &= SST'_{mod} - SST'_{obs} \\ &= SST_{mod} - \overline{SST_{mod}} - (SST_{obs} - \overline{SST_{obs}}) \\ &= X - \bar{X} \end{aligned}$$

The new constraint C_2 (Equation A.1.2) relies on two relaxation coefficients associated to two relaxation timescales: $\lambda_1$for the high frequencies and λ_2 for the low frequencies.

$$C_2 = -\lambda_1(X - \bar{X}) - \lambda_2\bar{X} \qquad \text{(A.1.2)}$$

The constraints in Equations A.1.1 and A.1.2 are effectively heat flux corrections (in Wm^{-2}), and the relaxation coefficients have units of $Wm^{-2}K^{-1}$.

A.2 Stability analysis of the SST constraint

Section A.1 of the Appendix introduced the formulation of the two-timescale SST constraint in Equation A.1.2. Using the operator $\mathcal{M}$ which represents the integration of the model from time *t* to time *t+1* and assuming that the SST constraint from Equation A.1.2 has been applied at time *t*, we have

$$SST_{t+1}^{mod} = \mathcal{M}\left(SST_t^{mod}\right) - \mu_1(X_t - \overline{X_t}) - \mu_2\overline{X_t}\,. \qquad \text{(A.2.1)}$$

where

$$\overline{X_t} = \frac{1}{N}\sum_{i=0}^{N-1} X_{t-i},$$

and

$$\mu_i = \frac{\lambda_i \Delta t}{\rho_0 C_p \Delta z}, \qquad i = 1,2. \qquad \text{(A.2.2)}$$

with C_p the ocean specific heat (in $J\,K^{-1}kg^{-1}$), ρ_0 the reference volumic mass of sea water (density in $kg\,m^{-3}$), Δt the length of a model time step (in seconds), Δz the thickness of the first ocean model layer (in meters) and $\lambda_{i=1,2}$ (in $W\,m^{-2}K^{-1}$) is the relaxation coefficient defined in Section A.1 and set before the coupled model integration.

The modelled SST at time *t* can be decomposed as,

$$\begin{aligned} SST_t^{mod} &= SST_t^{obs} + SST_t^{mod} - SST_t^{obs} + \varepsilon \\ &= SST_t^{obs} + X_t + \varepsilon, \end{aligned}$$

where ε combines the model and the observation errors. The notation ε stands for the general error in the following.

Equation A.2.2 thus becomes,

$$SST_{t+1}^{obs} + X_{t+1} = \mathcal{M}\left(SST_t^{obs} + X_t\right) - \mu_1(X_t - \overline{X_t}) - \mu_2\overline{X_t} + \varepsilon\,. \qquad \text{(A.2.3)}$$

A first order approximation for the term $\mathcal{M}\left(SST_t^{obs} + X_t\right)$ allows reformulating Equation A.2.3 as

$$SST_{t+1}^{obs} + X_{t+1} = \mathcal{M}\left(SST_t^{obs}\right) + \frac{\partial \mathcal{M}}{\partial SST}\left(SST_t^{obs}\right)X_t - \mu_1(X_t - \overline{X_t}) - \mu_2\overline{X_t} + \varepsilon\,.$$

Assuming now that the effect of the model $\mathcal{M}$ is negligible between two time steps,

$$\mathcal{M}\left(SST_t^{obs}\right) = SST_{t+1}^{obs},$$

and that $\mathcal{M}$ is constant,

$$\frac{\partial \mathcal{M}}{\partial SST}\left(SST_t^{obs}\right) \approx 1,$$

Equation A.2.3 can finally be written as

$$X_{t+1} = X_t - \mu_1(X_t - \overline{X_t}) - \mu_2\overline{X_t} + \varepsilon, \qquad \text{(A.2.4)}$$

where ε is the general error term in the system.

Equation A.2.4 means that the difference between the model SST and observations (SST error) at time $t+1$ depends on the difference at time t corrected by the SST constraint at time t described in Equation A.1.2. Equation A.2.4 can be seen as a N-dimensional autoregressive model of order 1 and can be written as a simple vector-matrix product:

$$Y_{t+1} = AY_t + \varepsilon\,, \qquad \text{(A.2.5)}$$

where $Y_t = [X_t, X_{t-1}, \ldots, X_{t-N}]$, ε is the error, and where the elements of the square matrix A (dimension N) are given by

$$A = \begin{bmatrix} a & b & \cdots & \cdots & b \\ 1 & 0 & \cdots & \cdots & 0 \\ 0 & \ddots & \ddots & & \vdots \\ \vdots & \ddots & \ddots & \ddots & \vdots \\ 0 & \cdots & 0 & 1 & 0 \end{bmatrix},$$

with

$$a = 1 - \mu_1 + \frac{(\mu_1 - \mu_2)}{N}\,,$$

and

$$b = \frac{(\mu_1 - \mu_2)}{N}\,.$$

The stability of the system of Equation A.2.5 will be affected by the choice of the relaxation coefficients. This stability can be investigated by estimating the eigenvalues of the matrix A. The eigenvalues are calculated through a simple Python routine where we assume $\Delta z = 10m$ and $\Delta t = 1$day and $N = 31$ (for 31 days).

The stability of the system of Equation A.2.5 depends on the modulus of the eigenvalues of the matrix A. The system becomes unstable and unsuitable for our purposes if there are eigenvalues whose modulus is greater than or equal to 1. This criterion implies that the relaxation coefficient $\mu_1 = 0$ has to be avoided as well as the combination of a strong μ_1 and a weak μ_2 (expressed as λ_1 and λ_2 following Equation A.2.2 on Figure 11a). Both cases are anyway not consistent with the purpose of the two-timescale SST constraint in which we will use a rather weak (but not null) μ_1 (λ_1) combined to a relatively strong μ_2 (λ_2).

Complex eigenvalues of the matrix A lead to oscillatory solutions for Equation A.2.5. The purpose of the SST constraint being to damp the SST errors with respect to the observations, it is necessary to avoid high-frequency oscillations in the constraint that would contaminate the damped SST signal. The matrix A can be diagonalised and, considering only the matrix vector product (the error ε being white noise), Equation A.2.5 can be written:

$$Y_{t+1} = AY_t = P^{-1}\,\Theta P Y_t\,,$$

where P is the matrix containing the eigenvectors and Θ is the diagonal matrix containing the eigenvalues of A. Using the transformation $Z_t = PY_t$, we obtain

$$Z_{t+1} = \Theta Z_t\,. \qquad \text{(A.2.6)}$$

For each eigenvalue θ_j (of modulus lower than 1), Equation A.2.6 describes a simple exponential decay system,

$$z_{t+1}^j = \theta_j z_t^j\,,$$

with

$$\theta_j = |\theta_j| e^{-i\omega_j t}.$$

Complex eigenvalues θ_j have an oscillation period T_j such as:

$$T_j = \frac{2\pi}{\omega_j}$$

The time needed by the SST constraint to attenuate the initial signal by half is here referred to as the time decay T_{dec} and is given by

$$T_{dec} = \frac{\ln 2}{\ln|\theta_j|}\,.$$

Our criteria for the choice of the relaxation coefficients $\mu_1$and μ_2 are i) to avoid growing eigenvalues $|\theta_j| > 1$ and ii) that the period of the oscillations T_j for complex eigenvalues should be larger than the time decay T_{dec}. The diagnostic of Figure 11b shows that this situation is mostly avoided when the values of μ_1 (λ_1) and μ_2 (λ_2) are moderate and/or close to each other.

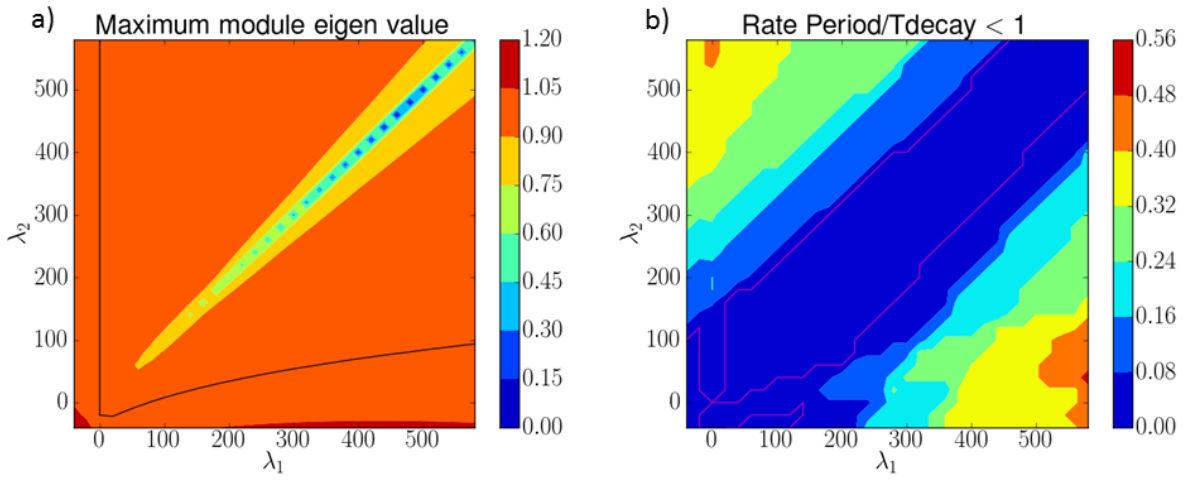

Figure 11a) Maximum modulus of the eigenvalues of the system described by Equation A.2.6 according to the relaxation coefficients $\boldsymbol{\lambda_1}$ *and* $\boldsymbol{\lambda_2}$ *(in* $\boldsymbol{W\ m^{-2}K^{-1}}$*). The black contour is the boundary between moduluses lower and higher than 1; b) ratio of eigenvalues producing oscillations with a period lower than the time decay* $\boldsymbol{T_{dec}}$ *according to the values of* $\boldsymbol{\lambda_1}$ *and* $\boldsymbol{\lambda_2}$*. A small ratio means that all the complex eigenvalues generate oscillations whose period is larger than the time decay* $\boldsymbol{T_{dec}}$*. The closer we are to a null ratio the better it is.*

Aknowledgments

The first version of the CERA system was developed within the two years of the CERA project (April 2012 to April 2014). The CERA project was funded by the European Spatial Agency (ESA) and part of their Data Assimilation projects (ESA-DA). The EU-funded ERA-CLIM2 project has since taken over the new developments for the CERA system.

REFERENCES

Bentamy, A., S. A. Grodsky, B. Chapron, and J. A. Carton, 2013. Compatibility of C- and Ku-band scatterometer winds: ERS-2 and QuikSCAT, J. Marine. Sys., Volumes 117–118, May 2013, Pages 72–-80. DOI: http://dx.doi.org/10.1016/j.jmarsys.2013.02.008

Caltabiano, A. C. V., Robinson, I. S., and Pezzi, L. P., 2005. Multi-year satellite observations of instability waves in the Tropical Atlantic Ocean, Ocean Sci., 1, 97-112, doi:10.5194/os-1-97-2005.

Chelton, Dudley B., et al., 2001. Observations of coupling between surface wind stress and sea surface temperature in the eastern tropical Pacific. Journal of Climate, 14.7, 1479-1498.

Chelton, D. B., Schlax, M. G., Freilich, M. H., & Milliff, R. F., 2004. Satellite measurements reveal persistent small-scale features in ocean winds. Science, *303*(5660), 978-983.

Gentemann, C. L., F. J. Wentz, C. A. Mears and D. K. Smith, 2004. In Situ Validation of Tropical Rainfall Measuring Mission Microwave Sea Surface Temperatures, J. Geophys. Res., 109, C04021, doi:10.1029/2003JC002092.

Ham, Y. G., & Kang, I. S. (2011). Improvement of seasonal forecasts with inclusion of tropical instability waves on initial conditions. Climate Dynamics, 36(7-8), 1277-1290.

Hashizume, H., S.-P. Xie, W. T. Liu, and K. Takeuchi (2001), Local and remote atmospheric response to tropical instability waves: A global view from space, J. Geophys. Res., 106(D10), 10173–10185, doi:10.1029/2000JD900684.

Inness, P. M., Slingo, J. M., Guilyardi, E., & Cole, J., 2003. Simulation of the Madden-Julian Oscillation in a coupled general circulation model. Part II: The role of the basic state. Journal of Climate, *16*(3), 365-382.

Kim, W., S.-W. Yeh, J.-H. Kim, J.-S. Kug, and M. Kwon, 2011. The unique 2009–2010 El Niño event: A fast phase transition of warm pool El Niño to La Niña, Geophys. Res. Lett., 38, L15809, doi:10.1029/2011GL048521.

Laloyaux, P, M. Balmaseda, D. Dee, K. Mogensen, P. Janssen, 2015. The ECMWF prototype for a coupled assimilation system. Submitted to Quarterly Journal of the Royal Meteorological Society

Mogensen, K., M. Alonso Balmaseda, A. Weaver, 2012. The NEMOVAR ocean data assimilation system as implemented in the ECMWF ocean analysis for System 4. ECMWF Technical Memoranda No 668, February 2012

Pedlosky, J., 2003. Waves in the ocean and atmosphere: introduction to wave dynamics. Springer Science & Business Media.

Rayner, N. A., Parker, D. E., Horton, E. B., Folland, C. K., Alexander, L. V., Rowell, D. P. and A., Kaplan, 2003. Global analyses of sea surface temperature, sea ice, and night marine air

temperature since the late nineteenth century. Journal of Geophysical Research: Atmospheres (1984–2012), 108(D14).

Seo, H., Jochum, M., Murtugudde, R., Miller, A. J., & Roads, J. O., 2007. Feedback of tropical instability-wave-induced atmospheric variability onto the ocean. Journal of Climate, 20(23), 5842-5855.

Shinoda, T., Kiladis, G. N., & Roundy, P. E., 2009. Statistical representation of equatorial waves and tropical instability waves in the Pacific Ocean. Atmospheric research, 94(1), 37-44.

Shinoda, T., 2012. Observation of first and second baroclinic mode Yanai waves in the ocean. Q.J.R. Meteorol. Soc., 138: 1018–1024. doi: 10.1002/qj.968

Vitart, F., & Molteni, F., 2010. Simulation of the Madden–Julian oscillation and its teleconnections in the ECMWF forecast system. Quarterly Journal of the Royal Meteorological Society, 136(649), 842-855.

Wheeler, M., & Kiladis, G. N., 1999. Convectively coupled equatorial waves: Analysis of clouds and temperature in the wavenumber-frequency domain. Journal of the Atmospheric Sciences, 56(3), 374-399.

Willett, C. S., Leben, R. R., & Lavín, M. F., 2006. Eddies and tropical instability waves in the eastern tropical Pacific: A review. Progress in Oceanography, 69(2), 218-238.

Wu, Q., & Bowman, K. P., 2007. Multiyear satellite observations of the atmospheric response to Atlantic tropical instability waves. Journal of Geophysical Research: Atmospheres (1984–2012), 112(D19).